Research Report

2001-07

Design and 3D Electromagnetic Field Analysis of Non-slotted and Slotted TORUS Type Axial Flux Surface Mounted Permanent Magnet Disc Machines

M. Aydin, S. Huang*, T.A. Lipo

*Department of Automation
Shanghai University
149 Yan-Chang Road
Shanghai, 200072, P.R. China

Wisconsin Power Electronic
Research Center
University of Wisconsin - Madison
Madison, WI 53703

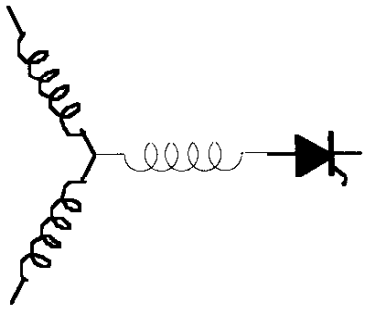

Wisconsin
Electric
Machines &
Power
Electronics
Consortium

University of Wisconsin-Madison
College of Engineering
Wisconsin Power Electronics Research Center
2559D Engineering Hall
1415 Engineering Drive
Madison WI 53706-1691

Design and 3D Electromagnetic Field Analysis of Non-slotted and Slotted TORUS Type Axial Flux Surface Mounted Permanent Magnet Disc Machines

Metin Aydin*
Student Member, IEEE

Surong Huang**

Thomas A. Lipo*
Fellow, IEEE

**Department of Automation
Shanghai University
149 Yan-Chang Road
Shanghai, 200072, P.R. China

*Department of Electrical and Computer Engineering
University of Wisconsin-Madison
1415 Engineering Drive
Madison, WI 53706-1691, U.S.A

Abstract: **Non-slotted and slotted external rotor internal stator TORUS type surface mounted permanent magnet (PM) machines (TORUS-NS and TORUS-S) have simple structures, relatively high efficiencies and low cost. These machines can be used for the applications that require high power and torque density, high efficiency and low noise with the use of Neodymium Iron Boron (NdFeB) magnets providing relatively small overall size and weight. In this paper, sizing equations of the TORUS machines are derived using generalized sizing equations. The optimum machine design is illustrated by choosing the magnet pole-arc ratio and the skew angle of the rotor magnets. Using the optimum design data, field analysis of TORUS-NS and TORUS-S machines are investigated. Pulsating torque analyses including the cogging torque and the ripple torque are carried out using a 3D Finite Element Analysis (FEA) software. Utilizing the techniques such as modifying the winding structure and skewing the rotor magnets, minimization of cogging torque and ripple torque for the TORUS-NS and TORUS-S machines are obtained and verified using 3D FEA. Finally a comparison of the TORUS topologies in terms of torque quality is illustrated in the paper.**

I. Introduction

TORUS machines are slotless or slotted, toroidal-stator, double rotor, axial type permanent magnet brushless machines. They have found a growing interest recently for high performance drive applications [1-2] and can be designed for higher torque-to-weight ratio, and higher efficiency.

General sizing equations can easily be applied to TORUS topologies and optimum machine design with high power/torque density, high efficiency, low noise and smooth torque can be achieved [3-4]. Pulsating torque is of importance for low noise and smooth torque applications for surface mounted PM machines. It comprises two components: cogging torque and ripple torque. Cogging torque arises from the variation of magnetic permeance of the stator teeth and the slots above the permanent magnets as the rotor rotates. The presence of cogging torque is a major concern in the design of permanent magnet machines since it adds unwanted harmonics to the pulsating torque.

Surong Huang has been supported by Wisconsin Power Electronics Research Center and Chinese National Science Foundation (59877014).

Ripple torque is mainly due to the fluctuations of the field distribution and the armature MMF which depends on the motor magnetic structure and the armature current waveform. Despite the fact that these torque components add unwanted harmonics to the pulsating torque, there exist certain techniques to minimize both cogging torque and ripple torque components of the disc-type machines.

The first section of this paper is devoted to introducing the non-slotted and slotted permanent magnet TORUS machine structures. The second section introduces sizing analysis and optimum design of the topologies using generalized sizing equations [5-6]. In the third section, FEA and calculations including field and torque analyses are presented and special attention is paid to torque ripple minimization using techniques such as using pie shaped winding structures, utilizing skewed rotor magnets. And lastly in the fourth section, the conclusions are summarized.

II. Torus Type Motor Structures

TORUS type disc machine has a single stator sandwiched between two disc rotors. The stator of the TORUS topology could be non-slotted (TORUS-NS) or slotted (TORUS-S). The TORUS-NS machine is a typical axial flux PM non-slotted motor structure. An idealized version of the machine structure is shown in Figure 1.

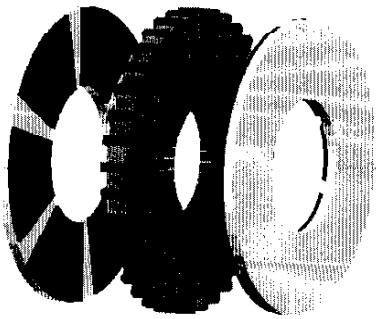

Fig. 1. TORUS-NS motor model

The machine has a single stator and two PM rotor discs. The stator of the machine is realized by tape wound core with AC

polyphase airgap windings which are wrapped around the stator core with a back-to-back connection. The rotor structure is formed by fan-shaped surface mounted NdFeB permanent magnets, rotor core and shaft. The two disc shape rotors carry the axially magnetized NdFeB magnets that they are mounted axially on the inner surfaces of the two rotor discs. Detailed views of the stator and rotor structures of the TORUS-NS machine are also given in Figure 2.

The portions between the windings are assumed to be filled with epoxy resin, as in all non-slotted structures, in order to increase the robustness and provide better conductor heat transfer. Moreover, the windings in the airgap are used for torque production. The end windings are quite short which results in making the copper loss of the machine smaller, efficiency higher and conductor heat transfer easier.

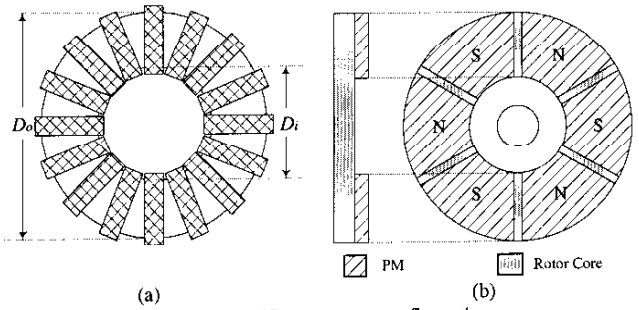

Fig. 2. TORUS type motor configuration
a) non-slotted stator structure b) rotor structure

The slotted TORUS motor structure is given in Figure 3. The machine has a stator structure with strip wound stator steel and two PM rotor discs. Evenly distributed back-to-back connected windings are placed into slots. The rotor structure is exactly the same as that of the TORUS-NS machine rotor as shown in Figure 2. The end windings are quite short which gives rise to higher efficiency for this topology.

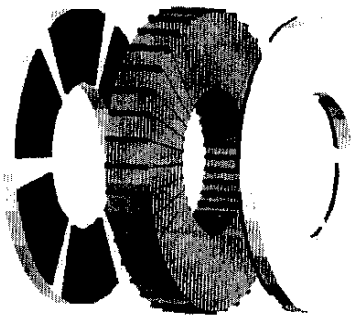

Fig. 3. TORUS-S motor model

The basic flux paths of the TORUS topologies analyzed in this paper at the average diameter are shown in Figure 4a and 4b for TORUS-NS and TORUS-S respectively. As can be seen from the figure, the N magnets drive flux into the stator core through the two airgaps. The flux then travels circumferentially along the stator core, returns across the airgaps and then enters the rotor core through the opposite polarity of the permanent magnets. Therefore, it can be expected that the axial length of the stator core would be quite long because of the summation of the flux entering the stator from both rotors.

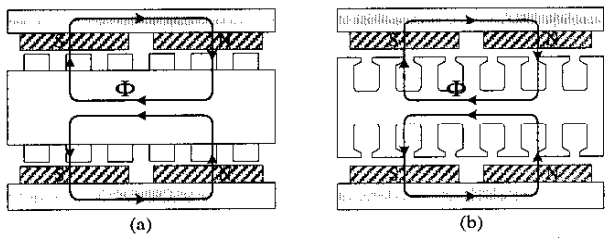

Fig. 4. One pole pair of the (a) TORUS-NS and (b) TORUS-S machines at the average diameter

III. Sizing Approach And Optimization Of The Torus Type Machines

A. Sizing Equations for the TORUS Topologies

The approach for the general purpose sizing equation has been provided in [5] and [6]. The sizing equations have the following form for axial flux machines (AFM) [6]:

$$P_R=\frac{1}{1+K_\phi}\frac{m}{m_1}\frac{\pi}{2}K_e K_i K_p K_L \eta B_g A \frac{f}{p}(1-\lambda^2)\frac{1+\lambda}{2}D_o^2 L_e \quad (1)$$

where

P_R — rated output power of the machine,
$K_\phi=A_r/A_s$ — ratio of electrical loading on rotor and stator (without a rotor winding, $K_\phi=0$),
m — number of machine phases,
m_1 — number of phases of each stator,
K_e — EMF factor
K_i — current waveform factor,
K_p — electrical power waveform factor,
η — machine efficiency,
B_g — air gap flux density,
A — total electrical loading,
f — converter frequency
p — machine pole pairs
L_e — effective stack length of the machine,
D_o, D_g, D_i — machine diameters at outer surface, air-gap surface and inner surface,
$K_L=D_o/L_e$ — aspect ratio coefficient for the AFM,
$\lambda=D_i/D_o$ — ratio of the diameter for the AFM.

The outer surface diameter D_o from (1)

$$D_o=\left(P_R/\frac{1}{1+K_\phi}\frac{m}{m_1}\frac{\pi}{2}K_e K_i K_p \eta B_g A \frac{f}{p}(1-\lambda^2)\frac{1+\lambda}{2}\right)^{1/3} \quad (2)$$

The machine total outer diameter D_t for the TORUS type machines is given as

$$D_t = D_o + 2W_{cu} \tag{3}$$

where W_{cu} is the protrusion of the end winding from the iron stack in the radial direction. For the back-to-back wrapped winding, protrusions exist toward the axis of the machine as well as towards the outside which can be calculated as

$$W_{cu} = \frac{D_i - \sqrt{(D_i^2 - 2A_s D_g)/\alpha_s K_{cu} J_s}}{2} \tag{4}$$

where α_s is the ratio of stator teeth portion to the stator pole pitch portion, for the non-slotted topology machines α_s=1.

The axial length of the machine L_e is

$$L_e = L_s + 2L_r + 2g \tag{5}$$

where L_s is axial length of the stator, L_r is axial length of the rotor and g is the air gap length.

The axial length of the stator L_s is

$$L_s = L_{cs} + 2\,W_{cu} \tag{6}$$

Note for the slotted topology machines the axial length of the stator slot L_{ss}=W_{cu}. The axial length of the stator core L_{cs} can be written as

$$L_{cs} = \frac{B_g\ \alpha_p\ \pi D_o(1+\lambda)}{B_{cs} 4\ p} \tag{7}$$

where B_{cs} is the flux density in the stator core and α_p is the ratio of average airgap flux density to peak airgap flux density.

The axial length of rotor L_r becomes

$$L_r = L_{cr} + L_{PM} \tag{8}$$

and the axial length of the rotor core L_{cr} is

$$L_{cr} = \frac{B_u\ \pi D_o(1+\lambda)}{B_{cr} 8p} \tag{9}$$

where B_u is the attainable flux density on the surface of the PM, B_{cr} is the flux density in the rotor disc core.

The PM length L_{PM} can be calculated as

$$L_{PM} = \begin{cases} \dfrac{\mu_r B_g}{B_r - B_g K_f / K_d}(g + W_{cu}) & \text{for TORUS-NS} \\ \dfrac{\mu_r B_g}{B_r - B_g K_f / K_d}(K_c\ g) & \text{for TORUS-S} \end{cases} \tag{10}$$

where μ_r is the recoil relative permeability of the magnet, B_r is the residual flux density of the PM material, K_d is the leakage flux factor, K_c is the Carter factor and K_f is the peak value corrected factor of air-gap flux density in radial direction of the disc motor.

B. Optimization of the TORUS Topologies

In axial flux machines, the ratio, λ, and airgap flux density are design parameters which have significant effect on the characteristic. Therefore, in order to optimize the machine performance, the ratio λ and the airgap flux density must be chosen carefully.

In Figure 5, power density is shown as a function of airgap flux density and the ratio λ for TORUS-NS machine. From this plot, the maximum power density (or torque density) occurs at an airgap flux density of 0.43 T and the diameter ratio of λ=0.454. The machine efficiency is 95.1% for that maximum power density point and close to the maximum efficiency point 95.6%. The design of the slotless machine at the maximum power density is also tabulated in Table I.

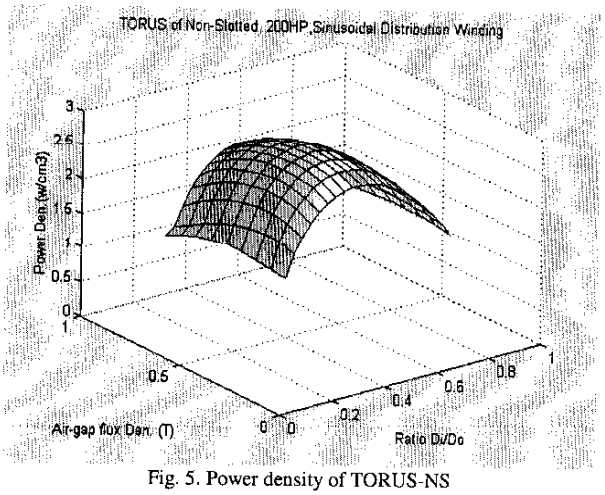

Fig. 5. Power density of TORUS-NS
vs. air-gap flux density (B_g) vs. diameter ratio (λ)
(P_R=200HP, n_s=1200rpm, p=3, A=600A/cm, J_s=9.0A/mm^2)

TABLE I

OPTIMIZATION OF THE TORUS-NS MACHINE FOR MAXIMUM POWER DENSITY POINT

Maximum power density (MPD)	P_{dmax}= 2.77 W/cm^3
Diameter ratio (λ) at MPD point	D_i/D_o=0.454
Airgap flux density at MPD point	B_g=0.43 T
Efficiency at MPD point	η = 95.1%

Optimization of the TORUS-NS machine can be achieved for the maximum efficiency point. The maximum efficiency occurs at a power density of 2.359 W/cm^3 and a ratio λ of 0.517. The airgap flux density at the maximum efficiency point is calculated to be 0.80T. Furthermore, the machine efficiency does not change significantly as the ratio λ changes.

Figure 6 shows power density plot as a function of airgap flux density and the ratio λ for TORUS-S machine. From this plot, the maximum power density, which is found as 2.56 W/cm^3, occurs at an airgap flux density of 0.91 T and the

diameter ratio of λ=0.460. For the maximum point, motor efficiency is found to be 94.9%. Power density and efficiency plots in 2D view are also illustrated for both TORUS-NS and TORUS-S machines in Figure 7 and the summary of the results are given in Table II.

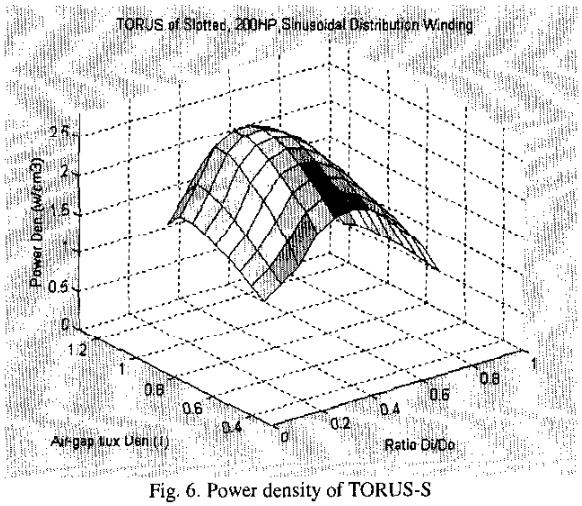

Fig. 6. Power density of TORUS-S
vs. air-gap flux density (B_g) vs. diameter ratio (λ)
(P_R=200HP, n_s=1200rpm, p=3, A=600A/cm, J_s=10.9A/mm^2)

TABLE II

OPTIMIZATION OF THE TORUS-S MACHINE FOR MAXIMUM POWER DENSITY POINT

Maximum power density (MPD)	P_{dmax}= 2.56 W/cm^3
Diameter ratio (λ) at MPD point	D_i/D_o=0.46
Airgap flux density at MPD point	B_g=0.91 T
Efficiency at MPD point	η = 94.9%

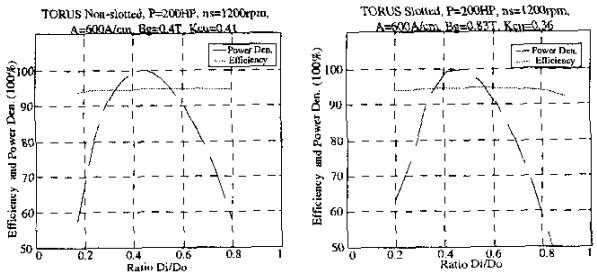

Fig. 7. 2D view of the power density and efficiency plots for both (a) TORUS-NS and (b) TORUS-S machines

IV. 3D FIELD ANALYSIS AND CALCULATIONS

A. Finite Element Analysis of Slotless TORUS Machine

To analyze the magnetic circuit and torque pulsations, 3D Finite Element Analysis was used for both TORUS machines. The purpose of the analysis is to realize an overall picture of the saturation levels in various parts of the machine, to compare the flux densities obtained from FEA and sizing analysis, and to investigate and minimize the cogging and ripple torque of the machines.

In TORUS-NS topology, the coil per pole per phase is chosen as 2 (q = 2 coils/pole/phase). In other words, there exist 36 back-to-back connected airgap windings around the stator. Also, it should be mentioned that sector shaped airgap windings are used in the model because they provide better utilization of the stator core and help to reduce the torque ripple of the machine. Finally, skewed rotor magnets are used in the model and the pole arc ratio, α_i, was selected as 0.8. The machine dimensions and parameters for TORUS-NS machine are tabulated in Table III.

TABLE III

PARAMETERS AND MACHINE DIMENSIONS OF TORUS-NS MACHINE

Frequency (f)	60 Hz
Number of poles (p)	6 poles
Surface current density (A)	600 A/cm
Current density (J_s)	9.0 A/mm^2
Airgap length (g)	0.1 cm
Pole-arc-ratio (α_i)	0.8
Outer diameter (D_o)	68.65 cm
Inner diameter (D_i)	31.13 cm
Slot depth (L_{ss})	0 cm
Axial length of stator core (L_{cs})	5.38 cm
Axial length of rotor core (L_{cr})	2.17 cm
Magnet axial length (L_{pm})	0.91 cm

Figure 8 shows the airgap flux density and flux paths for various parts of the machine for the no load case. From this plot it can be determined that the maximum flux density is roughly 0.45 Tesla and the average airgap flux density is about 0.36 T. A flux density comparison between the FEA results and sizing analysis results on various parts of the TORUS-NS machine at no load is tabulated in Table IV.

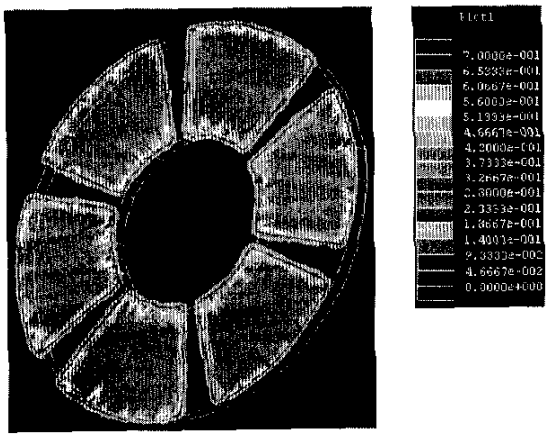

Fig. 8. Airgap flux density of the TORUS-NS machine at no load

TABLE IV

FLUX DENSITY COMPARISON OF TORUS-NS MACHINE AT NO LOAD

	Stator		Airgap		Rotor
	$B_{ts\text{-}max}$	$B_{cs\text{-}max}$	$B_{g\text{-}max}$	$B_{g\text{-}avg}$	$B_{cr\text{-}max}$
FEA	0	1.60	0.45	0.36	1.8
Sizing Eq	0	1.7	0.43	0.33	1.8

It is seen that the FEA results are consistent with the results obtained from the sizing analysis except for the fact that maximum value of the stator flux density is a little lower than the value obtained from sizing analysis. The reason for this discrepancy is that the leakage flux is a bit higher because of the large airgap which results in lower flux density in the stator core.

Figure 9 shows the airgap flux density over one pole using FEA. This curve shows that the flux density on the edges of the PM is about 20% higher than the flux density on the center of the PM because of the magnet leakage flux. Figure 10 illustrates how the airgap flux density of the TORUS-NS machine changes over one pole as the diameter varies from inner diameter D_i to outer diameter D_o.

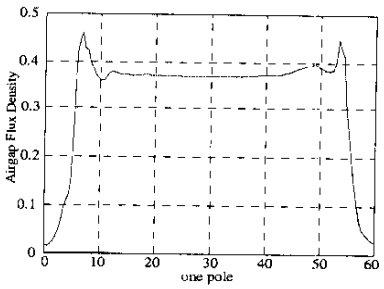

Fig. 9. No load airgap flux density of the TORUS-NS (at average diameter $D_g = (D_i + D_o)/2$)

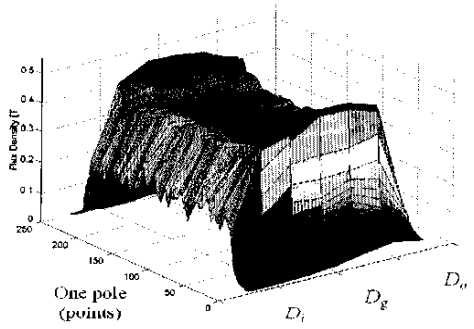

Fig. 10. No load airgap flux density of the TORUS-NS machine obtained from FEA (at D_i , D_g and D_o)

B. Finite Element Analysis of Slotted TORUS Machine

FEA of the TORUS-S machine was again realized for both no load and rated load cases. The parameters and machine dimensions used in the design which are calculated using sizing equations are shown in Table V. Figure 11 shows the airgap flux density of the machine for the no load case. It can be seen from these plots that the maximum airgap flux density is roughly 1.0 T and the average airgap flux density was determined to be 0.75 T.

TABLE V

PARAMETERS AND MACHINE DIMENSIONS OF TORUS-S MACHINE

Frequency (f)	60 Hz
Number of poles (p)	6 poles
Surface current density (A)	600 A/cm
Current density (J_s)	9.0 A/mm^2
Airgap length (g)	0.1 cm
Pole-arc-ratio (α_i)	0.8
Outer diameter (D_o)	51.96 cm
Inner diameter (D_i)	25.98 cm
Slot depth (L_{ss})	2.28 cm
Axial length of stator core (L_{cs})	8.91 cm
Axial length of rotor core (L_{cr})	5.06 cm
Magnet axial length (L_{pm})	1.20 cm

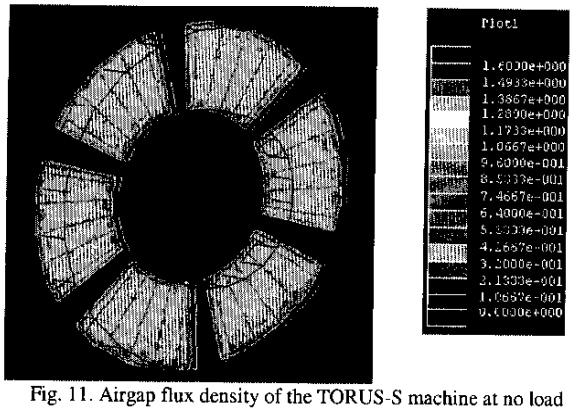

Fig. 11. Airgap flux density of the TORUS-S machine at no load

Using the principle of operation of the slotted TORUS machine, the magnetization directions of the magnets are set and the direction of the air gap flux density are illustrated in Figure 12 (a) while the flux directions in the stator of the machine at no load are shown in Figure 12 (b).

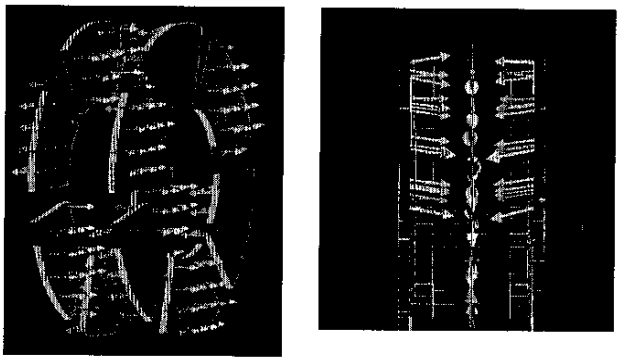

(a) (b)

Fig. 12. (a) Airgap flux density and (b) direction of the TORUS-S machine at no load

A comparison of the flux densities between the FEA results and sizing analysis results for different parts of the machine at no load is tabulated in Table VI. From the no load flux density plots, it is seen that the results are again consistent with the results obtained from the sizing analysis. The maximum flux density values on the rotor and stator were determined to be almost the same. Also, the maximum and average airgap flux densities obtained from the FEA and sizing analysis agree well.

TABLE VI

FLUX DENSITY COMPARISON OF TORUS-S MACHINE AT NO LOAD

	Stator		Airgap		Rotor
	$B_{ts\text{-}max}$	$B_{cs\text{-}max}$	$B_{g\text{-}max}$	$B_{g\text{-}avg}$	$B_{cr\text{-}max}$
FEA	1.75	1.7	1.0	0.75	1.8
Sizing	1.8	1.7	1.02	0.79	1.8

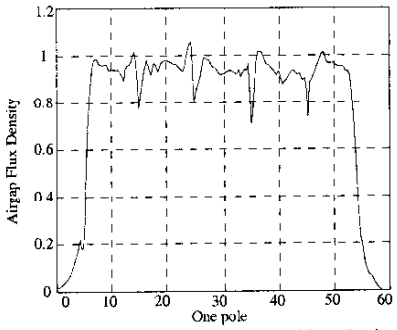

Fig. 13. Airgap flux density for TORUS-S machine obtained from FEA (at average diameter D_g)

The airgap flux density at the average diameter (D_g) over one pole using FEA was also obtained and is shown in Figure 13. This plot shows that there are gaps in the airgap flux density right above the stator slots arising from the fact that there is a sudden change of the airgap permeance because of the slots.

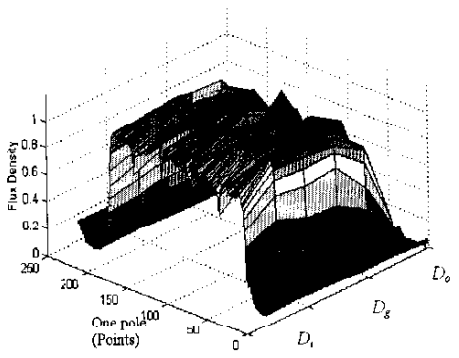

Fig. 14. 3D Airgap flux density for TORUS-S machine obtained from FEA

Magnetic wedges could be used to help to reduce the effects of the gaps, eliminate peaks and result in more smooth airgap flux density waveform. Figure 14 shows how the airgap flux density changes over one pole as the airgap diameter varies from inner (D_i) to outer (D_o).

V. TORQUE ANALYSIS USING FEA

In general, the total torque of a PM machine has three torque components: average torque, ripple torque and cogging torque. Since no slots exist in the TORUS-NS topology, the pulsating torque component of the machine is the same as the ripple torque component. However, in the TORUS-S topology, pulsating torque is comprised both cogging and ripple torque components.

A ripple torque analysis for the TORUS-NS machine was carried out using the Maxwell 3D software. FEA calculations were carried out for different rotor positions over one pole. The total torque of the machine at rated power without skewing the rotor PMs was plotted over one pole and is shown in Figure 15a. The peak-to-peak torque ripple was found to be 0.12 pu.

Several methods exist for reducing the torque ripple of a disc type permanent magnet machine. Changing the winding structure from a rectangular back-to-back connected structure to a pie shaped back-to-back structure and introducing skewed rotor magnets are some of these methods. As a second step of the analysis, the winding structure was changed to a pie shaped back-to-back structure and rotor magnets were skewed by the optimum skew angle, which was calculated to be 31 degrees and found that the MMF harmonics are minimized at this skew angle. The total torque plot was obtained so as to determine the torque ripple of the machine. The resultant plot is given in Figure 15b. As can be seen from the plot, the torque ripple was reduced to 0.046 pu.

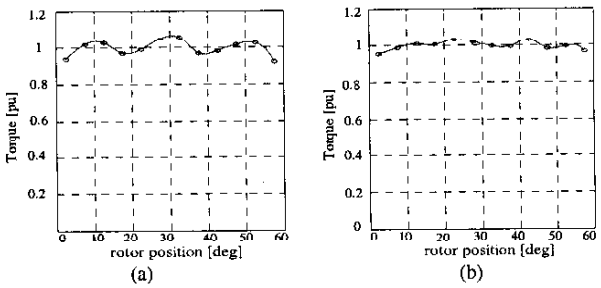

Fig. 15. Total torque of the TORUS-NS machine (a) without and (b) with skewed rotor magnets

The cogging torque analysis was also completed for two types of rotor structures for TORUS-S machine: without and with skewed PM rotor. The resultant plots are given in Figures 16a and 16b. As can be seen from the cogging torque plots, the peak-to-peak cogging torque for the TORUS-S topology without skewing the magnets is 6.2% of the rated torque. When the rotor magnets were skewed by 30 degrees, which is the optimum skew angle, the cogging became 1.3% of the rated torque. Therefore, skewing the rotor PMs reduced the cogging torque in this case by 79.0%.

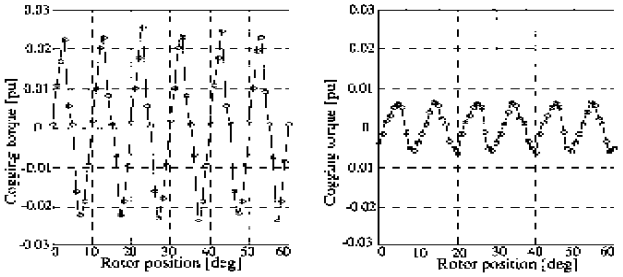

Fig. 16. Cogging torque of the TORUS-S machine (a) without and (b) with skewed rotor magnets

In order to obtain the total torque behavior of the TORUS-S machine, 3D Finite Element calculations were performed for different rotor positions for non-skewed and skewed magnet cases. The pulsating torques of both types were plotted over one pole and are shown in Figure 17a and 17b. The ripple torque of the machine was found as 0.156 pu peak-to-peak for the non-skewed rotor magnet case and 0.076 pu peak-to-peak for the skewed magnet rotor case. This results in a ripple torque reduction of 51.3% by simply skewing the magnets.

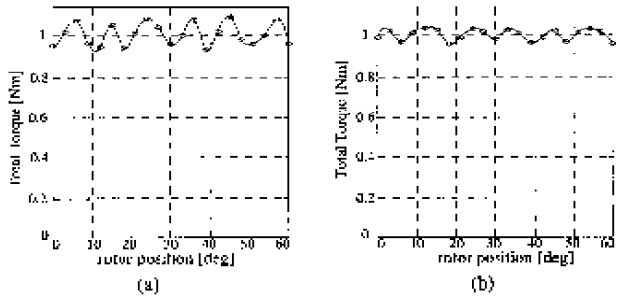

Fig. 17. Total torque of the TORUS-S machine at rated load (a) without and (b) with skewed rotor magnets

VII. Comparison And Conclusions

Within the selection and design of electric propulsion drive intended for high power/torque density, high efficiency, low noise and smooth torque applications, the focus of this paper was the analytical sizing, optimized machine design and torque quality for non-slotted and slotted TORUS type axial flux surface mounted PM machines. The key points of analytical sizing and optimized machine design are:

- In order to optimize the machine power density and efficiency, the ratio λ and the airgap flux density B_g must be chosen carefully.
- In order to minimize the ripple torque has to choose the magnet pole-arc ratio, the skew angle of the rotor magnets and winding distribution shape.
- Comparing non-slotted and slotted TORUS topologies, the non-slotted TORUS topology has negligible cogging torque and lower ripple torque than its slotted counterpart.

3D FEA models have been developed to yield reasonable predictions of the torque quality and 3D field distribution of both TORUS topologies. The machines are compared in terms of torque quality and the results are summarized in Table VII. The conclusions obtained from the FEA of both TORUS topologies with and without skewed rotor magnets are:

- For TORUS-NS machine, the peak-to-peak ripple torque reduction was found to be 61.7% by using pie shaped winding structure and skewed rotor magnets.
- The peak-to-peak ripple torque reduction was 51.3% for TORUS-S machine and the peak-to-peak cogging torque reduction was 79.0% by simply skewing the rotor magnets.

TABLE VII

RIPPLE TORQUE AND COGGING TORQUE COMPARISON FOR TORUS-S TOPOLOGIES

	Cogging Torque [pu]	Ripple Torque [pu]
TORUS-NS		
Without skewed rotor	0	0.12
With skewed rotor	0	0.046
TORUS-S		
Without skewed rotor	0.062	0.156
With skewed rotor	0.013	0.076

Acknowledgments

The authors are grateful to the Naval Surface Warfare Center for their financial support (Grant Number: N00014-98-1-0807).

References

[1] C. C. Jensen, F. Profumo and T. A. Lipo, "A Low Loss Permanent Magnet Brushless DC Motor Utilizing Tape Wound Amorphous Iron", IEEE Transactions on Industry Applications, Vol. 28, No. 3, May/June 1992, pp. 646-651.

[2] F. Profumo, Z. Zhang and A. Tenconi, "Axial Flux Machine Drive: New Viable Solution for Electric Cars", IEEE Transactions on Industrial Electronics, Vol. 44, No. 1, February1997, pp.39-45.

[3] T. A. Lipo, S. Huang and M. Aydin, "Performance Assessment of Axial Flux Permanent Magnet Motors for Low Noise Applications", Final Report to ONR, Oct 2000, Philadelphia.

[4] S Huang, M. Aydin and T. A. Lipo, "Comparison of (Non-slotted and Slotted) Surface Mounted PM Motors and Axial Flux Motors for Submarine Ship Drives", Third Naval Symposium on Electrical Machines, Dec. 2000.

[5] S. Huang, J. Luo, F. Leonardi, and T. A. Lipo, "A General Approach to Sizing and Power Density Equations for Comparison of Electrical Machines," IEEE Transactions on Industry Applications, IEEE Trans. IA-34, No.1, pp.92-97, 1998

[6] S. Huang, J. Luo, F. Leonardi and T. A. Lipo, "A Comparison of Power Density for Axial Flux Machines Based on the General Purpose Sizing Equation", IEEE Trans. on Energy Conversion, Vol.14, No.2 June 1999, pp. 185-192.